

# Hamiltonian learning of triplon excitations in an artificial nanoscale molecular quantum magnet

Rouven Koch,<sup>1</sup> Robert Drost,<sup>2</sup> Peter Liljeroth,<sup>2</sup> and Jose L. Lado<sup>2</sup>

<sup>1</sup>*QuTech and Kavli Institute of Nanoscience, Delft University of Technology, Delft 2628 CJ, The Netherlands*

<sup>2</sup>*Department of Applied Physics, Aalto University, 02150 Espoo, Finland*

Extracting the Hamiltonian of nanoscale quantum magnets from experimental measurements is a significant challenge in correlated quantum matter. Here we put forward a machine learning strategy to extract the spin Hamiltonian from inelastic spectroscopy with scanning tunneling microscopy, and we demonstrate this methodology experimentally with an artificial nanoscale molecular magnet based on cobalt phthalocyanine (CoPC) molecules on NbSe<sub>2</sub>. We show that this technique allows to directly extract the Hamiltonian parameters of a quantum magnet from the differential conductance, including the substrate-induced spatial variation of the different exchange couplings. Our methodology leverages a machine learning algorithm trained on exact quantum many-body simulations with tensor networks of finite quantum magnets, leading to a methodology that can be used to predict the Hamiltonian of CoPC quantum magnets of arbitrary size. Our results demonstrate how quantum many-body methods and machine learning enable learning a microscopic description of nanoscale quantum many-body systems with scanning tunneling spectroscopy.

Quantum magnets represent one of the potential platforms to create exotic quantum excitations [1, 2]. Quantum magnetism appears in Heisenberg models which are dominated by quantum fluctuations, an instance that often emerges in the presence of frustrated interactions [3–8]. These phenomena can give rise to a variety of excitations, including spinons, visons, gauge, and topological excitations [9–15]. This should be contrasted with classical symmetry broken magnets featuring magnon excitations [16–23]. Understanding the nature of excitations of a specific quantum material, thereby telling quantum from classical magnets, requires knowledge of the underlying Hamiltonian, which is often exceptionally difficult to extract from experiments [24].

Typical methodologies in quantum materials allow computing observables from Hamiltonians [25–27]. However, extracting the Hamiltonian from a set of observables is often a challenging problem for conventional techniques. Machine learning provides a strategy to tackle such a complex inverse problem beyond the reach of conventional methodologies in quantum materials. This has been demonstrated for Hamiltonian learning with supervised learning [28–30] and generative machine learning [31, 32], among others [26, 27, 33–36]. However, learning Hamiltonians in quantum magnets remains a relatively unexplored problem, which ultimately may allow tackling the open challenge of identifying the nature of quantum spin liquids.

Here we put forward a strategy to extract the underlying Hamiltonian from scanning tunneling microscopy (STM) measurements of a molecular quantum magnet. Our methodology relies on combining tensor-network many-body calculations of spin excitations of a molecular magnet with a machine learning methodology, which enables to extract the full Hamiltonian of the system directly from local inelastic tunneling spectroscopy measurements. The Hamiltonian learning algorithm can ex-

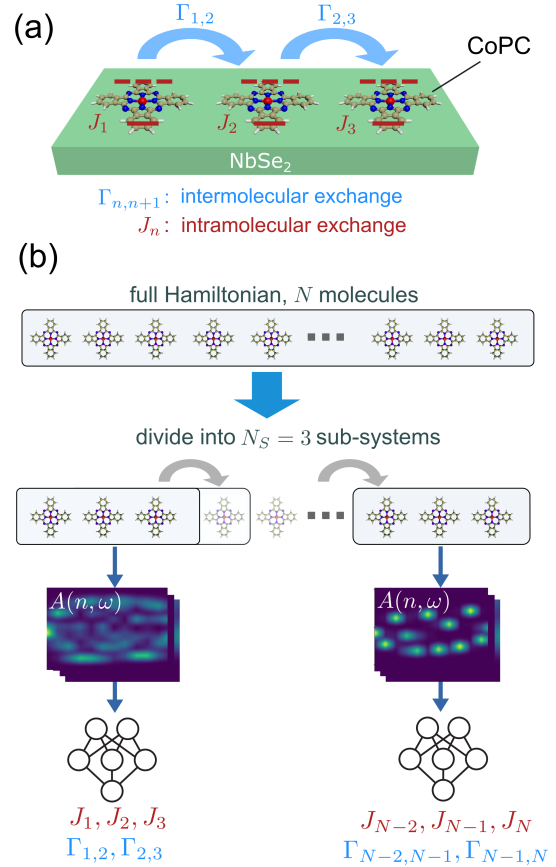


FIG. 1. (a) Schematic of the one-dimensional spin model hosting triplon excitations with intra- and intermolecular exchange parameters  $J$  and  $\Gamma$ . This system can be engineered in CoPC on NbSe<sub>2</sub>. (b) Machine learning workflow to extract Hamiltonian parameters of a chain of arbitrary length. Each site of the chain represents one CoPC molecule. The neural network predicts the spin Hamiltonian of Eq. 1.

tract spatially dependent Hamiltonian parameters for

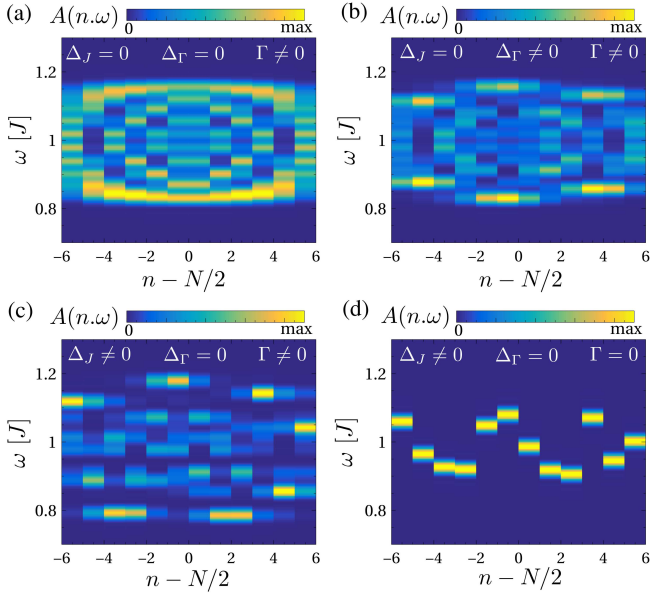


FIG. 2. Spectral function of the spin chain in the limit of no exchange nor coupling disorder (a), finite coupling disorder (b), finite exchange disorder (c), and fully decoupled molecules (d). It is observed that the presence of disorder and molecular coupling leads to a strongly featured spectral function. We took  $\Delta_J = 0.2J$ ,  $\Delta_\Gamma = 0.2J$ , and  $\Gamma = 0.3J$ , and the same identical disorder profile was used in (b-d).

arbitrarily large 1-dimensional molecular chains, solely by training the algorithm on many-body calculations of fixed-size systems. In particular, we demonstrate this methodology experimentally with a molecular quantum magnet hosting triplon excitations as realized in cobalt phthalocyanine (CoPC) molecules on NbSe<sub>2</sub>. Our methodology puts forward a strategy to characterize with atomic resolution Hamiltonians of quantum magnets, including capturing local variations of exchange parameters, establishing a machine-learning-enabled technique for Hamiltonian learning in molecular quantum nanomagnetism.

The system we focus on is a one-dimensional molecular quantum magnet that hosts triplon excitations and can be found experimentally in CoPC molecules on NbSe<sub>2</sub> (Fig. 1(a)) [37]. This system hosts two magnetic moments on two orbitals of the CoPC molecule, one in the center ion and the second distributed over the outer ligands [38]. The molecular chain realizes the following Hamiltonian

$$H = \sum_n J_n \mathbf{S}_n \cdot \mathbf{K}_n + \sum_n \Gamma_{n,n+1} \mathbf{S}_n \cdot \mathbf{S}_{n+1} \quad (1)$$

leading to a spin chain of length  $N$  with a pair of spin-1/2 operators  $\mathbf{K}_n = (\hat{K}_n^x, \hat{K}_n^y, \hat{K}_n^z)$  and  $\mathbf{S} = (\hat{S}_n^x, \hat{S}_n^y, \hat{S}_n^z)$  on each molecule  $n$ . The  $J_n$ 's are the intramolecular exchange couplings between the two orbitals and  $\Gamma_{ij}$  is the intermolecular exchange coupling between neigh-

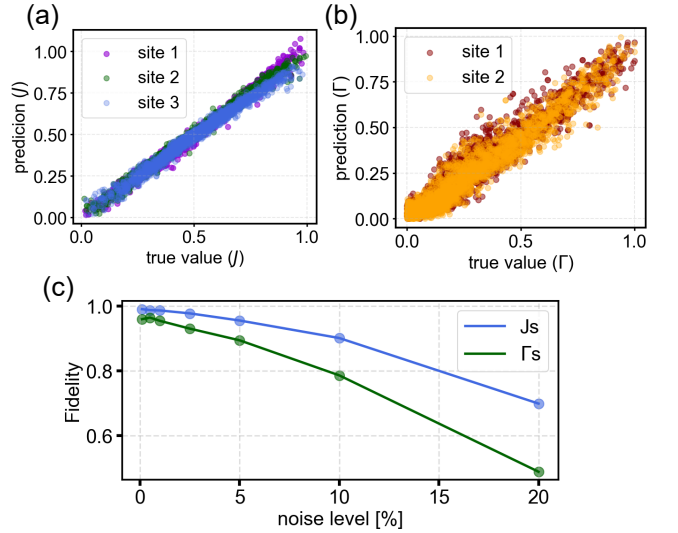


FIG. 3. Panels (a) and (b) show the predictions of the NN algorithm to extract the intra- and intermolecular exchange amplitudes described in Eq. 1 with the algorithm described in the Method section for 2% noise. The inputs of the model are the  $dI/dV$  spectra. Panel (c) shows the fidelity (defined in Eq. 5) vs. noise strength (defined in Eq. 4) for increasing noise.

boring molecules  $n$  and  $m$ . In general, the molecular chain will have average exchange couplings  $J = \langle J_n \rangle$  and  $\Gamma = \langle \Gamma_{n,n+1} \rangle$ , and random fluctuations of  $\Delta_J$  and  $\Delta_\Gamma$  around those averages. Triplons emerge in this system for  $J \gg \Gamma$ , where the bandwidth of the triplon excitations scales as  $\sim \Gamma$ , and their gap as  $\sim J$  [37]. The spectra of triplon excitations are accessed through the spectral function

$$A(n, \omega) = \sum_{\alpha=x,y,z} \langle GS | \hat{K}_n^\alpha \delta(\omega - \hat{H} + E_{GS}) \hat{K}_n^\alpha | GS \rangle \quad (2)$$

of the many-body ground state, that we compute using a tensor network kernel polynomial formalism [39–42]. Inelastic spectroscopy on the molecule with STM measurements [12, 16, 43–47] allows to directly access the previous spectral function as given by [48]

$$A(n, \omega) \propto d^2 I / dV^2. \quad (3)$$

Typical spectra on the different sites of a molecular chain are shown in Fig. 2, where we show the limit of a pristine molecular chain  $\Delta_J = 0$  (Fig. 2a), disorder in the coupling  $\Delta_\Gamma \neq 0$  (Fig. 2b), disorder in the internal exchange  $\Delta_J \neq 0$  (Fig. 2c), and a disordered decoupled chain with  $\Gamma = 0$ ,  $\Delta_J \neq 0$  (Fig. 2d). We observe that while both types of disorders  $\Delta_J$  and  $\Delta_\Gamma$  create fluctuations in the triplons, their relative values are challenging to directly extract from the spectral function.

Our objective is to develop a machine learning algorithm that is trained on a finite system size that directly generalizes to smaller and larger systems to extract the

Hamiltonian of the molecular quantum magnet. The goal of our algorithm is to learn the underlying intra- and intermolecular exchange parameters,  $J_n$  and  $\Gamma_{n,n+1}$ , by extracting information from the spectral functions that directly maps to  $dI/dV$  measurements. For this, we develop an iterative workflow with a deep neural network (NN) as the central part to infer the Hamiltonian parameters. We create a training set of molecular chains of length  $N = 12$  (24 spins  $S = 1/2$ ) with random Hamiltonian parameters  $J_n$  and  $\Gamma_{n,n+1}$ . We choose  $N = 12$  to take a moderately large system where finite size effects are not dominating. Then, we separate the Hamiltonian of Eq. 1 into sub-systems of length  $N_S = 3$  as depicted in Fig. 1(b). The sub-system has five Hamiltonian parameters, three  $J_n$  and two  $\Gamma_{n,n+1}$ . The NN algorithm predicts these five parameters at a time, taking the three  $dI/dV$ s (or spectral functions) of the sub-system molecules as inputs. Finally, the algorithm sweeps iteratively through the whole system of arbitrary size in slices of  $N_S = 3$  molecules. These slices, however, contain information from the larger parent Hamiltonian. In addition, we average over the parameters of overlapping sites to obtain more accurate predictions. The workflow is illustrated in Fig. 1(b). This enables us to make predictions for chains of arbitrary lengths by training the algorithm only on systems of size  $N = 12$  which keeps the computational costs very low even for predictions of very large systems. Our methodology allows us to directly extract spatially-dependent fluctuations of the exchange coupling, as emerging from stacking dependent exchange in experimental molecular systems [37]. In total, we create 1500 systems with varying disorder strength of size  $N = 12$  that we split up into  $N_S = 3$  subsystems to train the NN to infer the underlying parameters. Furthermore, we add noise to the simulated  $dI/dV$  spectra in the form of

$$\left(\frac{dI}{dV}\right)_{\text{noise}} = \left(\frac{dI}{dV}\right)_{\text{data}} + \eta \cdot \mathbf{R} \quad (4)$$

where  $(dI/dV)_{\text{noise}}$  represents the noisy simulated differential conductance,  $(dI/dV)_{\text{data}}$  is the original simulated differential conductance data,  $\eta$  is the noise level, and  $\mathbf{R}$  is a random noise matrix uniformly distributed in  $[0, 1]$ . More details about the data modeling, creation of the dataset, and the post-processing of the experimental data can be found in the Supplementary Information (SI). The ML model that we use is a feed forward NN, trained with data from the many-body spin chain from Eq. 1, where we define the intra-molecular exchange  $J_n \in [0, 1]$  and inter-molecular exchange  $\Gamma_{n,n+1} \in [0, 0.4]$ . The ML algorithm with the underlying NN learns to predict the underlying Hamiltonian of a  $N_S = 3$ -molecule sub-Hamiltonian by taking three dynamical correlators or  $dI/dV$  spectra as inputs, as depicted in Fig. 1(b). While being trained on sub-systems of the  $N = 12$ -molecule chain, the algorithm transfers to smaller and

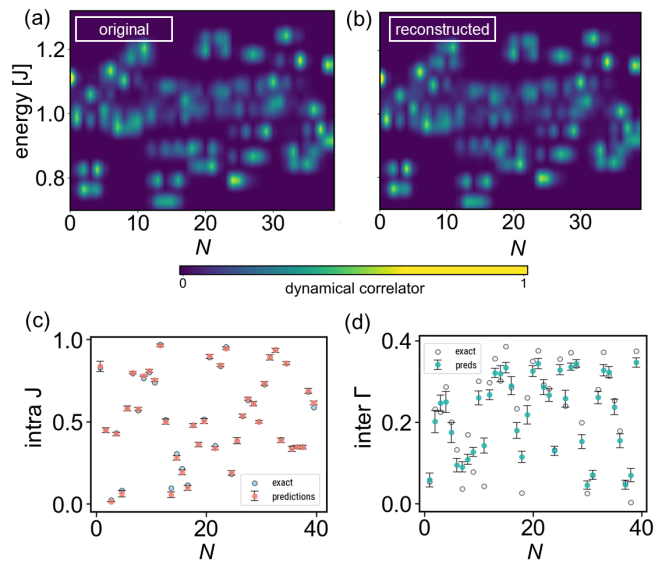


FIG. 4. Hamiltonian learning algorithm trained on systems of size  $N = 12$  applied to a simulated molecular chain of size  $N = 40$ . Panels (a) and (b) show the original and reconstructed dynamical correlator. Panels (c) and (d) the extracted and exact Hamiltonian parameters for the intra- and intermolecular exchange. The predictions are averaged over 10 random initializations of the NN.

larger system sizes without decreased precision. The details of the algorithm can be found in Ref. [49].

### Triplon excitations in a quantum magnet

In Fig. 3, we demonstrate the performance of the ML algorithm on the test data of the  $N = 12$  many-body model (for added noise of 2%). We compare the predictions of the intra-molecular  $J_n$  (a) and inter-molecular  $\Gamma_{n,n+1}$  exchange in Fig. 3(b) with their true value. The test samples are divided into sub-Hamiltonians of size  $N_S = 3$ . We observe that the algorithm predicts the intra-molecular exchange  $J_n$  in Fig. 3(a) with high accuracy, showing small deviations from the ideal match and a mean absolute error (MAE) of  $\mathcal{E}_J = 0.024$ . The predictions of the inter-molecular exchange  $\Gamma_{n,n+1}$  Fig. 3(b) show similar behavior, with slightly higher deviations from the ideal match and an increased MAE of  $\mathcal{E}_\Gamma = 0.051$ . The intramolecular exchange  $J_n$  determines the position of the excitation spectra and the intermolecular exchange  $\Gamma_{n,n+1}$  determines the width. The difference in accuracy of the predictions is related to the higher complexity and impact of  $\Gamma_{n,n+1}$  on the shape and features of the molecular chain.

The quality of the Hamiltonian extraction can be characterized by the fidelity between the prediction and the real exchange couplings defined as [28]

$$\begin{aligned}
F(\Lambda_{\text{pred}}, \Lambda_{\text{true}}) &= \\
&= \frac{|\langle \Lambda_{\text{pred}} \Lambda_{\text{true}} \rangle - \langle \Lambda_{\text{pred}} \rangle \langle \Lambda_{\text{true}} \rangle|}{\sqrt{(\langle \Lambda_{\text{true}}^2 \rangle - \langle \Lambda_{\text{true}} \rangle^2) (\langle \Lambda_{\text{pred}}^2 \rangle - \langle \Lambda_{\text{pred}} \rangle^2)}} \quad (5)
\end{aligned}$$

where  $\Lambda_{\text{true}} = J_n^{\text{true}}, \Gamma_{n,n+1}^{\text{true}}$  and  $\Lambda_{\text{pred}} = J_n^{\text{pred}}, \Gamma_{n,n+1}^{\text{pred}}$  are the true and predicted Hamiltonian parameters of the system. The fidelity is defined in the interval  $\mathcal{F} \in [0, 1]$  where 1 stands for identical predictions and true values and 0 for fully uncorrelated values. In Fig. 3(c), we show the resilience of the algorithm to noise added to the data. Fig. 3(c) shows that even for high noise levels of more than 10%, the fidelity of the intra- and intermolecular exchange remains high. As expected from the results of Fig. 3(a,b), the predictions for the intramolecular exchange have generally higher fidelity.

Now, we demonstrate that our algorithm is capable of extending to significantly longer spin chains. We apply the algorithm that is trained on systems of size  $N = 12$  to a simulated  $N = 40$  molecular spin chain with randomly chosen  $J_n$  and  $\Gamma_{n,n+1}$  and predict the underlying Hamiltonian, divided into  $N_S = 3$ -molecule sub-systems. In Fig. 4(a,b), we compare the calculated spectral function with the reconstructed one and show the difference in predictions for the intra- and intermolecular exchange in Fig. 4(c,d). We find that we can extract the intramolecular exchange with very high precision and a significantly lower error than the intermolecular exchange. These results are in accordance with the findings for the  $N = 12$  molecule systems of Fig. 3(a,b) where we discuss that  $\Gamma_{n,n+1}$  has a significantly lower impact on the spectral function and  $dI/dV$  compared to  $J_n$  and, therefore, is inherently more difficult to determine regardless of the method. However, the appearance of the reconstructed molecular chain Fig. 4(b) is almost indistinguishable from the original calculation Fig. 4(a) that is used as input to infer the Hamiltonian. This highlights that  $J$  has the greatest impact on the main features of the dynamical correlators (and  $dI/dV$ ). These results demonstrate that our algorithm is capable of extending to significantly longer chains and gives faithful results for arbitrarily long chains.

#### Application of the algorithm to experimental molecular chain

We now apply the algorithm to real measurement data for a one-dimensional molecular chain. The sample was fabricated by subliming CoPc molecules onto a freshly cleaved NbSe<sub>2</sub> substrate. Subsequently, the sample was transferred to a low-temperature STM operating at 4 K. The measurements were performed with a NbSe<sub>2</sub>-coated superconducting tip to enhance the energy resolution

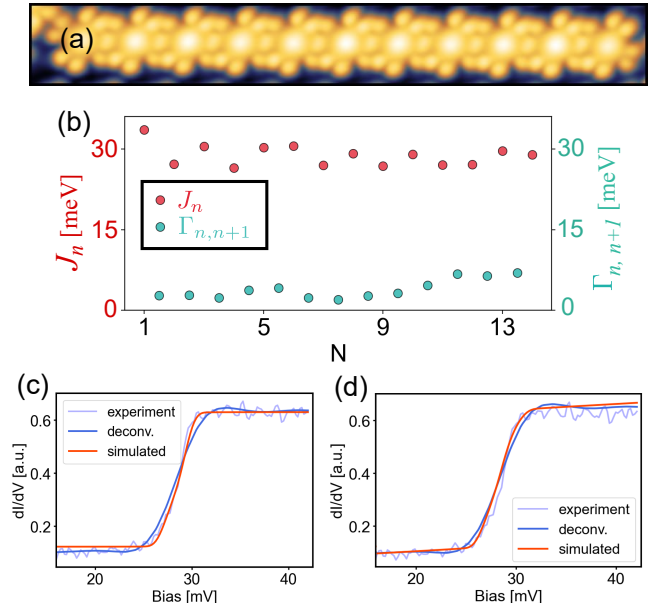


FIG. 5. (a) Image of a CoPC molecular chain on NbSe<sub>2</sub> (size  $20 \times 3 \text{ nm}^2$ ). (b) Extracted  $J_n$  and  $\Gamma_{n,n+1}$  for the  $N = 14$  molecular chain. (c,d) Hamiltonian extraction and reconstructed  $dI/dV$  from STM measurements. The examples are taken from  $dI/dV$  spectra from the chains with  $N = 14$  (c) and  $N = 11$  molecules (d). The experimental and deconvolved spectra are compared to the reconstructed simulated  $dI/dV$ .

[50–52]. This induces sharp peaks at the edges of the spin-flip excitations. The spectra can be deconvolved with the tip spectral density to remove this effect (details are given in the SI). Depending on the surface coverage, CoPC self-assembles into various motifs on NbSe<sub>2</sub>, forming individual molecules, molecular chains, and islands [37].

We now use our machine learning methodology to the experimental molecular chain. A typical STM image of such a system is shown in Fig. 5(a). In Fig. 5(b), we show the results of the Hamiltonian learning algorithm applied to the  $N = 14$  molecular chain, specifically enabling the extraction of the intra- and intermolecular exchange couplings for each molecule on the chain. In Fig. 5(c,d), we show example spectra from the measured triplon chains of lengths  $N = 14$  and  $N = 11$ , respectively. The Hamiltonian parameters are extracted from the deconvolved  $dI/dV$  spectra. We compare the reconstructed  $dI/dV$  spectra with the experimental and deconvolved spectra[53]. The results demonstrate that the weight of the step, which is proportional to the exchange coupling constant ( $J_n$ ), is accurately captured in panels Fig. 5(c,d). Furthermore, the width and steps, which are related to the broadening parameter ( $\Gamma_{n,n+1}$ ), are also well reproduced for both chains ( $N = 14, 11$ )[54]. For the intermolecular exchange ( $\Gamma_{n,n+1}$ ), we obtain values

of  $\Gamma \sim 0.08 - 0.19J$ , depending on the system size and specific molecule, consistent with previous average estimates [37]. These findings highlight that training the ML model with simulated data generalizes effectively to experimental data, eliminating the need for re-training, and is capable of predicting Hamiltonian parameters in systems whose system size is different from the theoretical training set. As a result, our algorithm is system-size independent and can be applied to experimental systems of arbitrary size, provided  $N > 3$ .

To summarize, here we presented a machine learning strategy to extract the underlying Hamiltonian of one-dimensional molecular spin systems. This methodology was demonstrated using a molecular spin chain hosting triplon excitations, highlighting its ability to extract information of 1D chains of arbitrary length by dividing the system into sub-Hamiltonians. Our methodology performs a faithful Hamiltonian extraction across a wide range of systems, from those with no disorder to highly disordered configurations. We showed that by solely training our algorithm in chains with  $N = 12$  molecules, the machine learning method enables us to perform Hamiltonian learning in systems of arbitrary size, in particular with  $N = 40$  emulated molecular spin chains. We applied our strategy for Hamiltonian learning to experimental  $dI/dV$  measurements of molecular quantum magnets, where we show accurate results in extracting Hamiltonians in disordered systems in the presence of noise in chains up to  $N = 14$  molecules. This strategy allows us to train the algorithm to work with arbitrary system sizes using quantum many-body calculations of specific finite-size systems. This approach can be extended to general spin models beyond those featuring triplons and general one-dimensional many-body Hamiltonians, possibly even to more spatial dimensions. Our results establish a versatile framework to perform Hamiltonian learning in engineered molecular quantum magnets, which can be extended to generic quantum lattice models, including interacting quantum dots or qubit arrays.

**Acknowledgments:** This research made use of the Aalto Nanomicroscopy Center (Aalto NMC) facilities and was supported by the Academy of Finland Projects Nos. 331342, 358088, 368478, 353839, and 347266, the Finnish Quantum Flagship, ERC grant (GETREAL, 101142364), and the KIND synergy program from the Kavli Institute of Nanoscience Delft. We thank S. Kezilebieke for help during the early stages of this project. We acknowledge the computational resources provided by the Aalto Science-IT project.

---

[1] Subir Sachdev, “Quantum magnetism and criticality,” *Nature Physics* **4**, 173–185 (2008).

- [2] Alexander Vasiliev, Olga Volkova, Elena Zvereva, and Maria Markina, “Milestones of low-d quantum magnetism,” *npj Quantum Materials* **3**, 18 (2018).
- [3] C. Broholm, R. J. Cava, S. A. Kivelson, D. G. Nocera, M. R. Norman, and T. Senthil, “Quantum spin liquids,” *Science* **367**, eaay0668 (2020).
- [4] Alexei Kitaev, “Anyons in an exactly solved model and beyond,” *Annals of Physics* **321**, 2–111 (2006).
- [5] Zhenyue Zhu, P. A. Maksimov, Steven R. White, and A. L. Chernyshev, “Topography of spin liquids on a triangular lattice,” *Phys. Rev. Lett.* **120**, 207203 (2018).
- [6] Shijie Hu, W. Zhu, Sebastian Eggert, and Yin-Chen He, “Dirac spin liquid on the spin-1/2 triangular Heisenberg antiferromagnet,” *Phys. Rev. Lett.* **123**, 207203 (2019).
- [7] Andrey V. Chubukov, T. Senthil, and Subir Sachdev, “Universal magnetic properties of frustrated quantum antiferromagnets in two dimensions,” *Physical Review Letters* **72**, 2089–2092 (1994).
- [8] Simeng Yan, David A. Huse, and Steven R. White, “Spin-liquid ground state of the  $s = 1/2$  kagome Heisenberg antiferromagnet,” *Science* **332**, 1173–1176 (2011).
- [9] Martin Mourigal, Mechthild Enderle, Axel Klöpperpieper, Jean-Sébastien Caux, Anne Stunault, and Henrik M. Rønnow, “Fractional spinon excitations in the quantum Heisenberg antiferromagnetic chain,” *Nature Physics* **9**, 435–441 (2013).
- [10] B. Dalla Piazza, M. Mourigal, N. B. Christensen, G. J. Nilson, P. Tregenna-Piggott, T. G. Perring, M. Enderle, D. F. McMorrow, D. A. Ivanov, and H. M. Rønnow, “Fractional excitations in the square-lattice quantum antiferromagnet,” *Nature Physics* **11**, 62–68 (2014).
- [11] Masanori Kohno, Oleg A. Starykh, and Leon Balents, “Spinons and triplons in spatially anisotropic frustrated antiferromagnets,” *Nature Physics* **3**, 790–795 (2007).
- [12] Shantanu Mishra, Gonçalo Catarina, Fupeng Wu, Ricardo Ortiz, David Jacob, Kristjan Eimre, Ji Ma, Carlo A. Pignedoli, Xinliang Feng, Pascal Ruffieux, Joaquín Fernández-Rossier, and Roman Fasel, “Observation of fractional edge excitations in nanographene spin chains,” *Nature* **598**, 287–292 (2021).
- [13] Wei Ruan, Yi Chen, Shujie Tang, Jinwoong Hwang, Hsin-Zon Tsai, Ryan L. Lee, Meng Wu, Hyejin Ryu, Salman Kahn, Franklin Liou, Caihong Jia, Andrew Aikawa, Choongyu Hwang, Feng Wang, Yongseong Choi, Steven G. Louie, Patrick A. Lee, Zhi-Xun Shen, Sung-Kwan Mo, and Michael F. Crommie, “Evidence for quantum spin liquid behaviour in single-layer 1T-TaSe<sub>2</sub> from scanning tunnelling microscopy,” *Nature Physics* **17**, 1154–1161 (2021).
- [14] Chenxiao Zhao, Gonçalo Catarina, Jin-Jiang Zhang, João C. G. Henriques, Lin Yang, Ji Ma, Xinliang Feng, Oliver Gröning, Pascal Ruffieux, Joaquín Fernández-Rossier, and Roman Fasel, “Tunable topological phases in nanographene-based spin-1/2 alternating-exchange Heisenberg chains,” *Nature Nanotechnology* **19**, 1789–1795 (2024).
- [15] Hao Wang, Peng Fan, Jing Chen, Lili Jiang, Hong-Jun Gao, Jose L. Lado, and Kai Yang, “Construction of topological quantum magnets from atomic spins on surfaces,” *Nature Nanotechnology* **19**, 1782–1788 (2024).
- [16] A. Spinelli, B. Bryant, F. Delgado, J. Fernández-Rossier, and A. F. Otte, “Imaging of spin waves in atomically designed nanomagnets,” *Nature Materials* **13**, 782–785 (2014).

- [17] D. R. Klein, D. MacNeill, J. L. Lado, D. Soriano, E. Navarro-Moratalla, K. Watanabe, T. Taniguchi, S. Manni, P. Canfield, J. Fernández-Rossier, and P. Jarillo-Herrero, “Probing magnetism in 2D van der Waals crystalline insulators via electron tunneling,” *Science* **360**, 1218–1222 (2018).
- [18] John Cenker, Bevin Huang, Nishchay Suri, Pearl Thijssen, Aaron Miller, Tiancheng Song, Takashi Taniguchi, Kenji Watanabe, Michael A. McGuire, Di Xiao, and Xiaodong Xu, “Direct observation of two-dimensional magnons in atomically thin CrI<sub>3</sub>,” *Nature Physics* **17**, 20–25 (2020).
- [19] David MacNeill, Justin T. Hou, Dahlia R. Klein, Pengxiang Zhang, Pablo Jarillo-Herrero, and Luqiao Liu, “Gigahertz frequency antiferromagnetic resonance and strong magnon-magnon coupling in the layered crystal crcl<sub>3</sub>,” *Phys. Rev. Lett.* **123**, 047204 (2019).
- [20] Wenyu Xing, Luyi Qiu, Xirui Wang, Yunyan Yao, Yang Ma, Ranran Cai, Shuang Jia, X. C. Xie, and Wei Han, “Magnon transport in quasi-two-dimensional van der Waals antiferromagnets,” *Phys. Rev. X* **9**, 011026 (2019).
- [21] D. Ghazaryan, M. T. Greenaway, Z. Wang, V. H. Guarochico-Moreira, I. J. Vera-Marun, J. Yin, Y. Liao, S. V. Morozov, O. Kristanovski, A. I. Lichtenstein, M. I. Katsnelson, F. Withers, A. Mishchenko, L. Eaves, A. K. Geim, K. S. Novoselov, and A. Misra, “Magnon-assisted tunnelling in van der Waals heterostructures based on CrBr<sub>3</sub>,” *Nature Electronics* **1**, 344–349 (2018).
- [22] Somesh Chandra Ganguli, Markus Aapro, Shawulienu Kezilebieke, Mohammad Amini, Jose L. Lado, and Peter Liljeroth, “Visualization of moiré magnons in monolayer ferromagnet,” *Nano Letters* **23**, 3412–3417 (2023).
- [23] A. V. Chumak, V. I. Vasyuchka, A. A. Serga, and B. Hillebrands, “Magnon spintronics,” *Nature Physics* **11**, 453–461 (2015).
- [24] Hidenori Takagi, Tomohiro Takayama, George Jackeli, Giniyat Khaliullin, and Stephen E. Nagler, “Concept and realization of Kitaev quantum spin liquids,” *Nature Reviews Physics* **1**, 264–280 (2019).
- [25] Eyal Bairey, Itai Arad, and Netanel H. Lindner, “Learning a local Hamiltonian from local measurements,” *Physical Review Letters* **122**, 020504 (2019).
- [26] Jianwei Wang, Stefano Paesani, Raffaele Santagati, Sebastian Knauer, Antonio A. Gentile, Nathan Wiebe, Maurangelo Petruzzella, Jeremy L. O’Brien, John G. Rarity, Anthony Laing, and Mark G. Thompson, “Experimental quantum Hamiltonian learning,” *Nature Physics* **13**, 551–555 (2017).
- [27] Valentin Gebhart, Raffaele Santagati, Antonio Andrea Gentile, Erik M. Gauger, David Craig, Natalia Ares, Leonardo Banchi, Florian Marquardt, Luca Pezzè, and Cristian Bonato, “Learning quantum systems,” *Nature Reviews Physics* **5**, 141–160 (2023).
- [28] Maryam Khosravian, Rouven Koch, and Jose L Lado, “Hamiltonian learning with real-space impurity tomography in topological moiré superconductors,” *Journal of Physics: Materials* **7**, 015012 (2024).
- [29] Greta Lupi and Jose L. Lado, “Hamiltonian learning quantum magnets with non-local impurity tomography,” *arXiv e-prints*, arXiv:2412.07666 (2024), arXiv:2412.07666.
- [30] Netta Karjalainen, Zina Lippo, Guangze Chen, Rouven Koch, Adolfo O. Fumega, and Jose L. Lado, “Hamiltonian inference from dynamical excitations in confined quantum magnets,” *Physical Review Applied* **20**, 024054 (2023).
- [31] Rouven Koch and Jose L. Lado, “Designing quantum many-body matter with conditional generative adversarial networks,” *Phys. Rev. Res.* **4**, 033223 (2022).
- [32] Rouven Koch, David van Driel, Alberto Bordin, Jose L. Lado, and Eliska Greplova, “Adversarial hamiltonian learning of quantum dots in a minimal Kitaev chain,” *Physical Review Applied* **20**, 044081 (2023).
- [33] Agnes Valenti, Guliuxin Jin, Julian Léonard, Sebastian D. Huber, and Eliska Greplova, “Scalable Hamiltonian learning for large-scale out-of-equilibrium quantum dynamics,” *Physical Review A* **105**, 023302 (2022).
- [34] Liangyu Che, Chao Wei, Yulei Huang, Dafa Zhao, Shunzhong Xue, Xinfang Nie, Jun Li, Dawei Lu, and Tao Xin, “Learning quantum Hamiltonians from single-qubit measurements,” *Physical Review Research* **3**, 023246 (2021).
- [35] James R. Garrison and Tarun Grover, “Does a single eigenstate encode the full Hamiltonian?” *Physical Review X* **8**, 021026 (2018).
- [36] Olivier Simard, Anna Dawid, Joseph Tindall, Michel Ferrero, Anirvan M. Sengupta, and Antoine Georges, “Learning interactions between Rydberg atoms,” (2024), arXiv:2412.12019 [quant-ph].
- [37] Robert Drost, Shawulienu Kezilebieke, Jose L. Lado, and Peter Liljeroth, “Real-space imaging of triplon excitations in engineered quantum magnets,” *Physical Review Letters* **131**, 086701 (2023).
- [38] Yuqi Wang, Soroush Arabi, Klaus Kern, and Markus Ternes, “Symmetry mediated tunable molecular magnetism on a 2d material,” *Communications Physics* **4**, 101 (2021).
- [39] Jose L. Lado, “<https://github.com/joselado/dmrgpy>,” .
- [40] Matthew Fishman, Steven R. White, and E. Miles Stoudenmire, “The ITensor Software Library for Tensor Network Calculations,” *SciPost Phys. Codebases*, 4 (2022).
- [41] Andreas Holzner, Andreas Weichselbaum, Ian P. McCulloch, Ulrich Schollwöck, and Jan von Delft, “Chebyshev matrix product state approach for spectral functions,” *Phys. Rev. B* **83**, 195115 (2011).
- [42] J. L. Lado and Oded Zilberberg, “Topological spin excitations in Harper-Heisenberg spin chains,” *Phys. Rev. Res.* **1**, 033009 (2019).
- [43] A. J. Heinrich, J. A. Gupta, C. P. Lutz, and D. M. Eigler, “Single-atom spin-flip spectroscopy,” *Science* **306**, 466–469 (2004).
- [44] Shawulienu Kezilebieke, Rok Žitko, Marc Dvorak, Teemu Ojanen, and Peter Liljeroth, “Observation of coexistence of Yu-Shiba-Rusinov states and spin-flip excitations,” *Nano Letters* **19**, 4614–4619 (2019).
- [45] R. Toskovic, R. van den Berg, A. Spinelli, I. S. Eliens, B. van den Toorn, B. Bryant, J.-S. Caux, and A. F. Otte, “Atomic spin-chain realization of a model for quantum criticality,” *Nature Physics* **12**, 656–660 (2016).
- [46] Deung-Jang Choi, Nicolas Lorente, Jens Wiebe, Kirsten von Bergmann, Alexander F. Otte, and Andreas J. Heinrich, “Colloquium: Atomic spin chains on surfaces,” *Rev. Mod. Phys.* **91**, 041001 (2019).
- [47] Kai Yang, William Paul, Fabian D. Natterer, Jose L. Lado, Yujeong Bae, Philip Willeke, Taeyoung Choi, Alejandro Ferrón, Joaquín Fernández-Rossier, Andreas J. Heinrich, and Christopher P. Lutz, “Tuning the ex-

- change bias on a single atom from 1 mT to 10 T,” *Phys. Rev. Lett.* **122**, 227203 (2019).
- [48] J. Fernández-Rossier, “Theory of single-spin inelastic tunneling spectroscopy,” *Phys. Rev. Lett.* **102**, 256802 (2009).
- [49] Rouven Koch, “Repository: MI-triplon-excitations,” (2025).
- [50] Shuai-Hua Ji, Tong Zhang, Ying-Shuang Fu, Xi Chen, Xu-Cun Ma, Jia Li, Wen-Hui Duan, Jin-Feng Jia, and Qi-Kun Xue, “High-resolution scanning tunneling spectroscopy of magnetic impurity induced bound states in the superconducting gap of Pb thin films,” *Phys. Rev. Lett.* **100**, 226801 (2008).
- [51] K. J. Franke, G. Schulze, and J. I. Pascual, “Competition of superconducting phenomena and Kondo screening at the nanoscale,” *Science* **332**, 940–944 (2011).
- [52] Shawulienu Kezilebieke, Marc Dvorak, Teemu Ojanen, and Peter Liljeroth, “Coupled Yu–Shiba–Rusinov states in molecular dimers on NbSe<sub>2</sub>,” *Nano Letters* **18**, 2311–2315 (2018).
- [53] Offset and absolute magnitude of the simulated data are adjusted to emulate the experimental spectra, as outlined in the SI.
- [54] As seen in Fig. 5(b), the predictions for the intermolecular exchange show a higher deviation. This is also the case for the experimental  $dI/dV$  spectra, i.e., the center of the step ( $J_n$ ) is predicted with high precision and the width and steps ( $\Gamma_{n,n+1}$ ) can deviate more, depending on the chain and specific measurement.

# Supplementary Information: Hamiltonian learning of triplon excitations in an artificial nanoscale molecular quantum magnet

Rouven Koch,<sup>1</sup> Robert Drost,<sup>2</sup> Peter Liljeroth,<sup>2</sup> and Jose L. Lado<sup>2</sup>

<sup>1</sup>*QuTech and Kavli Institute of Nanoscience, Delft University of Technology, Delft 2628 CJ, The Netherlands*

<sup>2</sup>*Department of Applied Physics, Aalto University, 02150 Espoo, Finland*

(Dated: April 30, 2025)

## DATA MODELING

The data preparation process is divided into two parts: (1) modeling of simulated data and (2) post-processing of experimental data prior to Hamiltonian extraction.

### Simulated data

The process of the data modeling for the simulated data is depicted in Fig. S1(a). First, we compute dynamical correlators using the Python library `dmrgpy`[1] for the Hamiltonian describing the molecular quantum magnet as defined in Eq.(1). We then perform a numerical integration to obtain the  $dI/dV$  spectra (panel (a)). The spectra are cropped to retain only the experimentally relevant region (15 to 45 meV), excluding the superconducting gap around zero sample bias. To apply our algorithm to the raw measurement data, we mimic experimental features including noise, an offset, and a linear background increase (panel (b)). For the application of the deconvolved  $dI/dV$  spectra shown in Fig. S1(d), we only add an offset to the simulations. We generate 1500 systems of size  $N = 12$  with intra-molecular exchange  $J \in [0, 1]$  and inter-molecular exchange  $\Gamma \in [0, 0.4]$ . For each sample, the offset is varied to capture realistic experimental conditions and add variety to the training data set.

### Experimental data

**(1) Predictions for deconvolved  $dI/dVs$ .** For the experimental data, an example measurement is shown in Fig. S1(c). The  $dI/dV$  spectra are normalized and deconvolved to remove the effects of the NbSe<sub>2</sub>-coated superconducting tip. The extraction of the Hamiltonian parameter for the  $N = 14$  molecule chain is shown in Fig. 5(b) and example plots are shown in Fig. 5(c,d).

**(2) Predictions for original  $dI/dVs$ .** In Fig. S2, we apply the algorithm to the (normalized) raw  $dI/dV$  spectra. In addition to the offset, we add a linear increase and additional noise to our simulations to model the measurement data. The modeling process is shown in Fig. S1(a,b). In Fig. S2, we show examples of the reconstructed simulations vs. the original, not deconvolved, spectra, taken from molecules on the 11- and 14-molecule chain. We crop the bias interval to 15 – 45 meV and neglect the superconducting gap. The predictions show similar precision as the application of the algorithm on the deconvolved spectra.

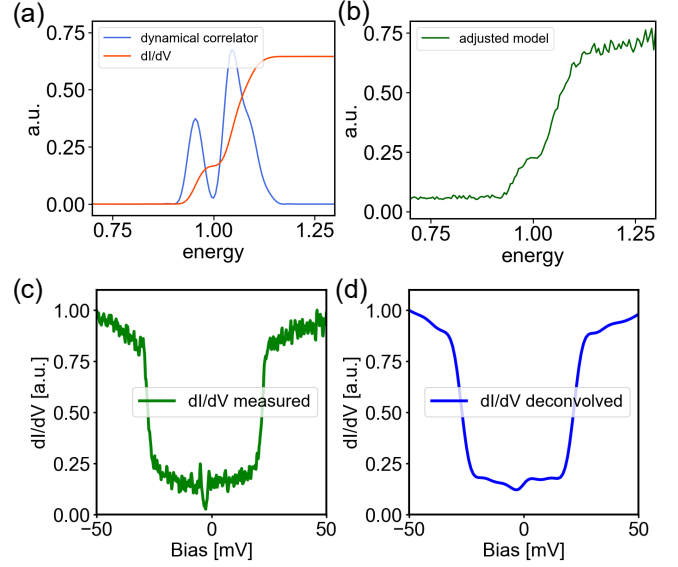


Fig. S1. Example of the data modeling for the simulated data and post-processing of experimental data. Panel (a) shows the dynamical correlator for a Hamiltonian of the form of Eq.(1) and the differential conductance ( $dI/dV$ ), and (b) shows the adjusted model with added noise, an offset, and a linear increase to mimic experimental data. (c) Example of the normalized experimental  $dI/dV$  from the  $N = 14$  chain and (d) post-processed deconvolved  $dI/dV$ .

## Experimental Details

To create the quantum magnet, we sublime the CoPc molecules under ultrahigh vacuum (UHV) onto a freshly cleaved NbSe<sub>2</sub> substrate. The sample was then immediately transferred to a low-temperature STM operating at 4 K in UHV where  $dI/dV$  spectra were acquired. The measurements were performed with a NbSe<sub>2</sub>-coated superconducting tip [2]. Depending on the surface coverage, CoPc self-assembles into various motifs, forming individual molecules, molecular chains, and islands.

The CoPc molecule exhibits two distinct adsorption sites on this surface [3]. Depending on the alignment between the high-symmetry axes of the molecule and the substrate, it can exhibit either spin-flip excitations or Yu-Shiba-Rusinov states [2–5]. For engineering quantum magnets and novel phases from a  $S = 0$  ground state, we focus only on those molecules featuring spin-flip excitations. The spin moments arise from two unpaired elec-

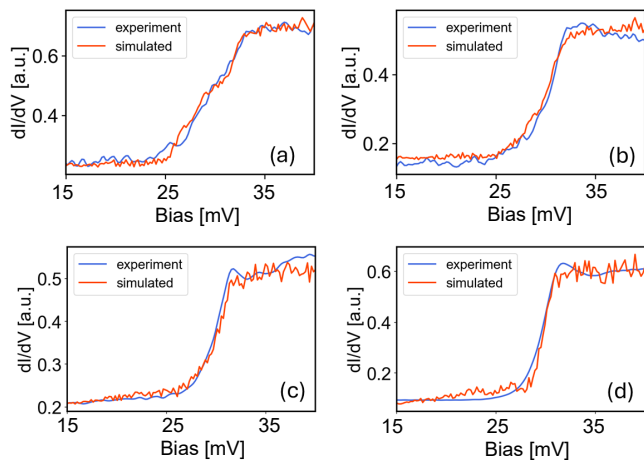


Fig. S2. (a-d) show examples for the predicted (simulated) spectrum from the original (experimental)  $dI/dV$  spectra from the  $N = 11, 14$  molecule chains. In this case, the algorithm is applied to the not deconvolved and post-processed  $dI/dV$  spectra.

trons occupying distinct molecular orbitals in CoPC. One of these orbitals is centered on the metal ion and the other one on the peripheral carbon atoms. The differential conductance can be obtained with STM measurements and has two dominating features (see Fig. S1(c)). The first one is the superconducting gap close to zero bias and can be related to the NbSe<sub>2</sub> substrate. The second feature

is sharp peaks at higher energy that can be related to inelastic spin-flip excitations when a tunneling electron excites the singlet state into a triplet state [2, 6, 7]. The resolution of the measurements can be enhanced by using a NbSe<sub>2</sub>-coated superconducting tip [2] that induces sharp peaks at the edges of the spin-flip excitations.

- 
- [1] Jose L. Lado, “<https://github.com/joselado/dmrgpy>,” .
  - [2] Shawulienu Kezilebieke, Marc Dvorak, Teemu Ojanen, and Peter Liljeroth, “Coupled Yu–Shiba–Rusinov states in molecular dimers on NbSe<sub>2</sub>,” *Nano Letters* **18**, 2311–2315 (2018).
  - [3] Yuqi Wang, Soroush Arabi, Klaus Kern, and Markus Ternes, “Symmetry mediated tunable molecular magnetism on a 2d material,” *Communications Physics* **4**, 101 (2021).
  - [4] Shawulienu Kezilebieke, Rok Žitko, Marc Dvorak, Teemu Ojanen, and Peter Liljeroth, “Observation of coexistence of Yu–Shiba–Rusinov states and spin-flip excitations,” *Nano Letters* **19**, 4614–4619 (2019).
  - [5] Markus Ternes, “Spin excitations and correlations in scanning tunneling spectroscopy,” *New Journal of Physics* **17**, 063016 (2015).
  - [6] A. J. Heinrich, J. A. Gupta, C. P. Lutz, and D. M. Eigler, “Single-atom spin-flip spectroscopy,” *Science* **306**, 466–469 (2004).
  - [7] Cyrus F. Hirjibehedin, Christopher P. Lutz, and Andreas J. Heinrich, “Spin coupling in engineered atomic structures,” *Science* **312**, 1021–1024 (2006).